Journal of the European Ceramic Society 19 (1999) 2285–2296

PII: S0955-2219(99)00118-1
0955-2219/99/$ - see front matter

Creep of SiC–SiC Microcomposites

Kevin L. Rugg,[a]* Richard E. Tressler,[a] Charles E. Bakis[b] and Jacques Lamon[c]

[a]Department of Materials Science and Engineering, The Pennsylvania State University, University Park, PA 16802, USA
[b]Department of Engineering Science and Mechanics, The Pennsylvania State University, University Park, PA 16802, USA
[c]Laboratoire des Composites Thermostructuraux, Domaine Universitaire, 33600 Pessac, France

Abstract

The creep behavior of SiC/C/SiC microcomposites at 1200–1400°C and 140–450 MPa was investigated in the presence and absence of matrix cracking. The microcomposites consisted of single Hi Nicalon or Carborundum fibers coated with a CVD carbon interlayer and a CVD SiC matrix. Since the fibers and matrix had been examined by the identical experimental technique, direct comparisons of the creep of the composite and of the constituents were performed. The creep of uncracked microcomposites was successfully modeled using a simple rule of mixtures algorithm. When matrix cracks were present, the microcomposites were modeled using a series composite consisting of intact microcomposite, exposed fiber at the matrix crack, and the debonded region in between. Trends for behavior with respect to the various mechanical and structural parameters that control creep are presented. © *1999 Elsevier Science Ltd. All rights reserved.*

Keywords: modelling, SiC-fibers, composites, creep, SiC.

1 Introduction

Ceramic matrix composites (CMCs) are being developed for use in high temperature structural applications. There are relatively few published reports about the creep of these materials.[1–11] Theoretical approaches to composite creep behavior are often based on a microcomposite unit consisting of a single fiber sheathed by a cylinder of the matrix material with or without an interlayer.[3,4,12–16] This simple unit cell has been used in experimental investigation of composite behavior. Chemical vapor deposited (CVD) SiC fibers have been considered as microcomposite structures in thermoelastic[17] and creep investigations.[15] The mechanical properties of composite interfaces have also been studied using microcomposite specimens.[18–20] In the present study, the interaction of these behaviors are presented. The creep of microcomposites is reported and the resulting behavior is modeled in the presence and absence of matrix cracking.

Creep in uncracked composites is controlled by stress transfer. The less creep resistant component (fiber or matrix) sheds load over time to the more creep resistant component. This change leads to the achievement of a nearly steady state creep rate due to the steady state creep of the more creep resistant component or to the failure of that component. In the case of an elastic fiber, creep halts when the matrix completely unloads onto the fiber. Chermant and Holmes[1] defined the creep mismatch ratio, $\mathrm{CMR} = \dot{\varepsilon}_f/\dot{\varepsilon}_m$ to categorize the type of creep behavior. For CMR less than 1, the matrix unloads onto the fiber and damage occurs by fiber failures. For CMR greater than 1, the fiber unloads onto the matrix and damage occurs by cavitation or cracking in the matrix. Creep of CMCs can fall into either regime.

Matrix cracking leads to increased loading on the fibers in the vicinity of the matrix crack. If the fibers have sufficient strength, the composite can continue to hold load until the creep rupture time of the fibers is exceeded. Following the initial matrix cracking, additional composite degradation can occur by several different mechanisms. Growth of the fiber/matrix interface debond can occur due to the difference in the radial creep strain of the fibers and that of the matrix.[13,16] In oxidizing environments, the interfacial properties (and hence the creep behavior) can be altered by removal of the interface layer or by closure of the interface by oxidation of the fiber and/or matrix. In multidimensional composites, matrix crack growth can occur through the 0° plies during composite creep.[11,21] For microcomposite tests in inert environments it has been demonstrated that none of these degradation mechanisms are important.[20]

*To whom correspondence should be addressed at current address: Rockwell Science Center, 1049 Camino Dos Rios, Thousand Oaks, CA 91361, USA.

2 Experimental Procedure

The single fiber microcomposites (shown schematically in Fig. 1) were produced at the Laboratoire des Composites Thermostructuraux (LCTS) using a process similar to that for manufacturing CVI composites.[22] Two SiC fibers were used, the 17 μm diameter (nominal) sintered α-SiC fiber from the Carborundum Company and the 14 μm polymer derived Hi Nicalon™ fiber (Nippon Carbon Company). These fibers were from the same batches as specimens used in earlier single fiber creep tests.[23] All microcomposites had a 0·1 μm pyrocarbon interlayer. The Carborundum microcomposites were received May 1995 and had a nominal matrix thickness of 5 μm. The individual test specimens with the Carborundum microcomposites are designated with the prefix 'C'. The Hi Nicalon microcomposites were received in four batches. The first received in May 1995, designated 'H5', had a matrix thickness of 5 μm, the second received in May 1996 had a matrix thickness of 10 μm and is designated 'H10', and the third and fourth batches received in August 1996 had a 3 μm matrix and are designated 'H3'. The H5-, H10-, and C- batches of microcomposites were fabricated by conventional CVD(CVI) while the H3- batch was prepared by pulsed CVD. It was determined that the matrix deposited on the microcomposites was Si-rich leading to poorer than expected creep properties.[24]

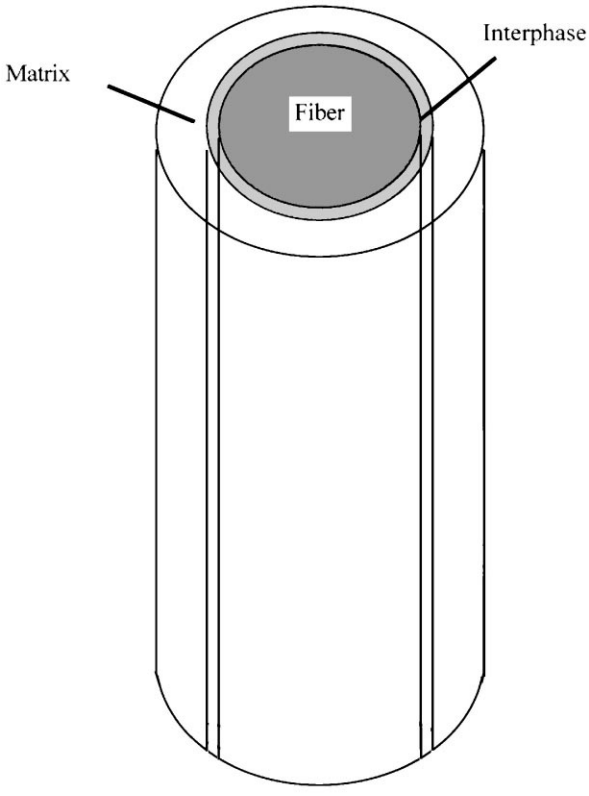

Fig. 1. Schematic of a microcomposite.

The microcomposites were cemented into 203 μm diameter alumina tubes using an alumina-based adhesive.* The tubes were sliced along 14 mm length to provide a long channel for adequate gripping. The specimen length between tubes was 15 ± 1 mm, equivalent to the hot zone of the furnace. The tubes were epoxied to steel washers for gripping outside the furnace. A few of the specimens which were tested at stresses below the matrix cracking stress were epoxied directly to the washers without use of the alumina tubes. The equivalence of the two gripping procedures was validated by demonstrating the consistency of the creep behavior of single Hi Nicalon fibers using both techniques. Creep tests were performed on a fiber testing apparatus described in detail elsewhere.[25] The specimen was suspended from a micropositioning motor, through a platinum/rhodium wound furnace, to a load cell. An encoder in the motor monitored the rotations of the drive gear which was converted to specimen strain. The entire test system was encased in a glass bell jar to allow controlled atmospheres. Unless otherwise indicated, all experiments were conducted in flowing argon. Due to thermal expansion effects, the apparatus required a 4 h dwell at temperature prior to the commencement of the experiments.

Creep tests were performed at temperatures between 1200 and 1400 °C and stresses between 100 and 450 MPa. All experiments commenced with a load–unload–reload hysteresis loop at temperature to check for the presence of matrix cracking and interfacial sliding. When matrix cracking was suspected, the microcomposite creep tests were periodically interrupted with hysteresis loops. The results of these hysteresis tests are reported elsewhere.[20] The matrix and fibers were tested individually on the same apparatus for direct comparison.[23,24]

The effective gauge length for creep, l_{geff}, is not well defined for microcomposites tested in a temperature gradient.[26] The CVI matrix has a lower creep activation energy than do the fibers,[23,24] therefore matrix creep strain accumulates over a longer length of the specimen in the furnace. The effective gauge length for matrix creep is therefore longer than that for fiber creep. For purposes of strain calculations in this paper, the effective gauge length for all microcomposites will be taken as 15 mm, the total length of the specimen between the tube grips. This is longer than that for the fibers [$l_{\mathrm{geff(fiber)}} \approx 10$ mm at the temperatures of interest] therefore for modeling and comparison purposes the creep rates of the fibers were multiplied by a

*Ceramabond 503, Aremco, Ossining, NY.

factor of $l_{\text{geff(fiber)}}/15$ to account for the shorter effective gauge length of the fibers.

3 Results and Discussion

3.1 Microcomposites without matrix cracks

The creep behavior of microcomposites was investigated with respect to a large number of control variables including fiber type, fiber volume fraction, applied stress, creep temperature, and matrix crack density. The conditions for individual creep tests are given in Table 1.

The creep behavior of uncracked microcomposites at 1300°C is compared to the behavior of single fibers and matrix specimens in Fig. 2. As discussed above, the fiber strains have been normalized to the microcomposite effective gauge length for comparison purposes. The fibers and matrix specimens were tested on the identical apparatus as the microcomposites were and followed the same experimental procedure. Specimen failures, when they occurred, are indicated in all figures, but most samples were removed from the test rig prior to failure for inspection. For microcomposites based on either fiber, the creep resistance of the microcomposite is between those of the fiber and matrix tested at the same stress and temperature. There is no creep curve shown for a Carborundum fiber at 100 MPa in Fig. 2 because that fiber does not show measurable creep strain at that stress at 1300 °C. Also plotted on each graph in Fig. 2 is the creep curve for a single fiber tested at an applied stress approximately equal to σ_{app}/V_f where σ_{app} is the remote stress on the microcomposite and V_f is the fiber volume fraction. This is equal to the stress that would be on the fiber in the microcomposite if the matrix carried no load. It is clear that the Hi Nicalon microcomposite creep strain is well below that for this fiber, however for the Carborundum microcomposite the creep strain is actually greater than that of the single fiber. The increased strain results from elastic strain of the fiber during creep due to stress transfer from the less creep resistant matrix. At longer times, the creep rate of the Carborundum fiber tested at σ_{app}/V_f is greater than that of the microcomposite.

Table 1. Microcomposite creep conditions

Specimen no.	V_f	*Precracking conditions*	*Temperature (°C)*	*Stress(es) (MPa)*	*Time (f) (h)*	*No. of cracks*
C-3	0·50	–	1400	140	96	0
C-4	0·50	–	1300	280	17·25(f)	0
C-5	0·33	–	1300	104	87	0
				22	24	
H10-7	0·28	–	1300	147	18·1	0
				222	2·2(f)	?
H10-9	0·20	Bending	1300	199	24	6
H10-10	0·17	Bending	1400	140	2·9(f)	?
H10-11	0·17	Bending	1200	134	15·6	?
				201	35	
H5-4	0·44	–	1300	130	24	0
				30	24	
H5-6	0·26	–	1300	423	1·04(f)	1
H5-7	0·27	Tension 532 MPa	1300	190	15	?
				266	24	
H5-9	0·27	Tension 600 MPa	1300	381	9·8(f)	3?
H5-10	0·28	Tension 500 MPa	1200	305	2	1
				375	2·5(f)	
H5-11	0·37	Tension 546 MPa	1250	436	8·3(f)	2–4
H3-1	0·45	Tension 840 MPa	1300	168	37	1?
H3-2B	0·48	–	1300	200	25	0
				25	52·5	
				200	25	
				25	25	
				200	25	
H3-4	0·44	–	1400	200	7(f)	0
H3-6A	0·48	–	1200	200	25·5	0
H3-7B	0·51	Tension 900 MPa	1200	200	50	7
H3-8	0·50	Tension 1·2 GPa	1200	450	24	21
H3-11A	0·52	–	1300	100	24	0
H3-12	0·48	–	1200	450	25	0

The creep of uncracked microcomposites was modeled using a simple rule of mixtures approach.[3,15] The model assumes no residual stresses, instantaneous loading, and perfect load transfer across the interface. The applied stress is initially distributed according to the elastic constants and volume fractions of the fiber and matrix. The stresses in each component change over time as the less creep resistant phase unloads onto the more creep resistant phase. Primary creep laws were used for modeling the creep behavior of the fiber and the matrix since these expressions are the best currently available,[23,27] although their use for complex load histories is probably inappropriate. The total creep strain of each constituent consists of an elastic and a creep component:

$$\varepsilon_{f,m} = \frac{\sigma}{E} + A\sigma^n t^p e^{-\frac{P}{T}} \quad (1)$$

where ε is the creep strain, σ is the applied stress, t is the time, T is the absolute temperature, E is the Young's modulus, n is the creep stress exponent, p is the creep time exponent, and $P = pQ/R$ where Q is the activation energy and R is the gas constant. The fiber and matrix parameters used in the calculations are given in Table 2.[23,24] Since the strain rates in each of the composite constituents are constrained to be equal, the change in stress in either constituent at any time can be derived. The fiber stress rate, for example, is[3]

$$\dot{\sigma}_f = -\frac{V_m E_f E_m}{V_f E_f + V_m E_m} \times \left[A_m \left(\frac{\sigma - V_f \sigma_f}{V_m} \right)^{n_m} t^{p_m} e^{\frac{-P_m}{T}} - A_f \sigma_f^{n_f} t^{P_f} e^{\frac{-P_f}{T}} \right]. \quad (2)$$

The change in constituent stress over a time interval Δt is calculated. The composite strain over that time interval is determined from

$$\varepsilon(t + \Delta t) = \varepsilon(t) + \left(\frac{\dot{\sigma}_f}{E_f} + A_f p_f \sigma^{n_f} t^{p_f - 1} \right) \Delta t. \quad (3)$$

The strain in eqn (3) can be calculated equally well using the matrix elastic and creep parameters. For the first iteration, the initial strains is simply the elastic strain of the composite computed from the rule of mixtures. The calculation [eqn (3)] is iterated as necessary until the conclusion of the simulation. The time interval Δt must be chosen small enough for the convergence to the same final solution yet large enough to avoid numerical instability at small times.

The creep behavior of microcomposites based on both SiC fibers at 100 MPa and 1300 °C is shown in Fig. 3. The fiber volume fraction for the Carborundum-based microcomposite was 0·33 while that for the Hi Nicalon microcomposite was 0·52. Porosity was negligible. The solid lines in the figure are the results of the rule-of-mixtures model. The prediction is excellent for both microcomposites. The

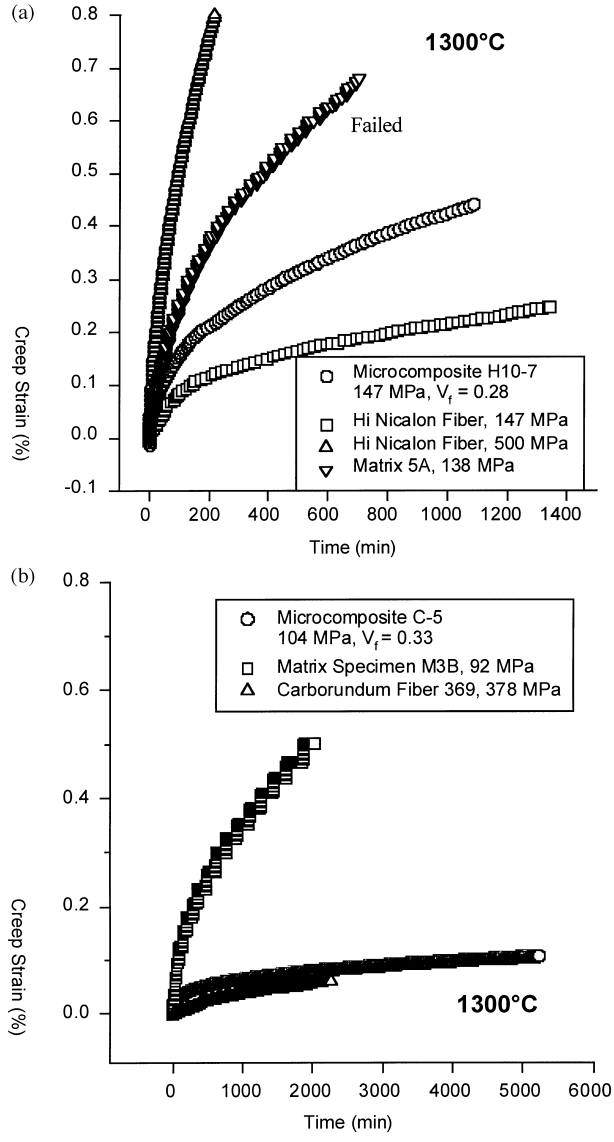

Fig. 2. Comparison of the creep curve for a (a) Hi Nicalon-based microcomposite and (b) a Carborundum-based microcomposite, a matrix sample, and fibers at 1300 °C. The creep curves of the fibers have been normalized to the microcomposite gauge length.

Table 2. Fiber and matrix creep properties used in composite creep models [22,23]

	A ($\text{min}^{-p}\ \text{Pa}^{-n}$)	p	n	$P(=pQ/R)$ (K)	E (GPa)
Matrix	$2{\cdot}33\times10^{-17}$	0·49	1·9	9607	420
Carborundum fiber[a]	$5{\cdot}10\times10^{-12}$	0·61	1·84	34 777	420
Hi Nicalon fiber[a]	$1{\cdot}94\times10^{-7}$	0·48	1·42	32 042	200

[a] Adjusted for change in gauge length.

Carborundum-based microcomposite has better creep resistance than the Hi Nicalon-based microcomposite as expected from the fiber creep results.

The evolution of the fiber and matrix stresses calculated from the rule of mixtures model is shown in Fig. 4. For the Carborundum-based microcomposite the stresses on both components start out equal since the fiber and matrix have the same elastic modulus. The fiber stress, σ_f, quickly increases to approximately 237 MPa while the matrix stress, σ_m, decreases to 38 MPa. For the Hi Nicalon microcomposites, the initial stress distribution is not equal. The matrix has a higher elastic modulus than does the fiber so the initial stress on the matrix is higher than that on the fiber (the strains must be equal). The elastic misfit stresses relax very quickly and it is reasonable to assume that if there were residual stresses in the microcomposite, they would also quickly dissipate as noted by Park and Holmes.[4] The matrix sheds load onto the fiber until $\sigma_f = 118$ MPa and $\sigma_m = 80$ MPa at the conclusion of the simulation. The matrix carries a significantly larger part of the applied stress for the Hi Nicalon microcomposite than for the Carborundum microcomposite in the figure. In both cases, the early stages of creep elongation are characterized by stress transfer to the creep resistant fibers, while the later stages can be thought of as nearly constant stress creep.

It is simple to use the rule of mixtures model to simulate the changes in the stress state during creep of microcomposites for which the matrix is the more creep resistant phase (CMR > 1) as might be expected for a stoichiometric matrix. Fig. 5 shows the fiber and matrix stresses for a theoretical Hi Nicalon-based microcomposite coated with a matrix that creeps at an order of magnitude lower rate than that observed. The rest of the conditions are identical to those of Fig. 4. The initial fiber and matrix stresses are the same as in the earlier case, but the matrix now accepts load shed from the fiber. The amount of stress transferred is low since the matrix stress is initially much higher than the fiber stress. Therefore, the creep strain arising from the elastic loading of the matrix in the initial stage of the simulated experiment is lower than in the CMR < 1 case.

The fiber volume fraction dependence of the creep curves for Hi Nicalon-based microcomposites at 1300° and 140 ± 10 MPa is shown in Fig. 6. The fiber volume fraction for specimen H10-7 is 0·28 while that of specimen H5-4 is 0·44. As can be anticipated from the CMR being less than one, the microcomposite with the greater fiber volume has

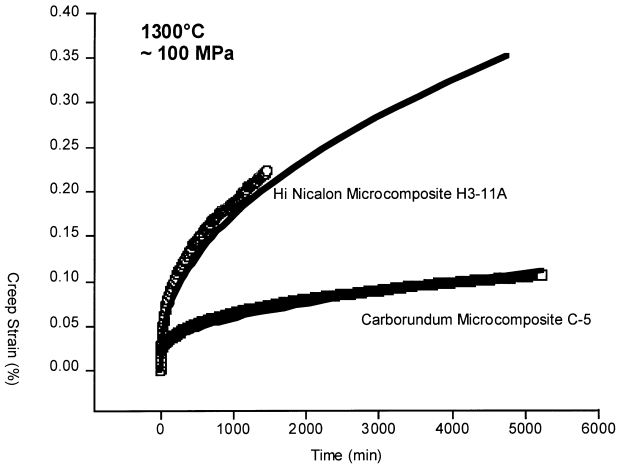

Fig. 3. Comparison of the creep behavior of Carborundum- and Hi Nicalon-based microcomposites. The experimental results are shown by the symbols and the rule of mixtures models by the lines.

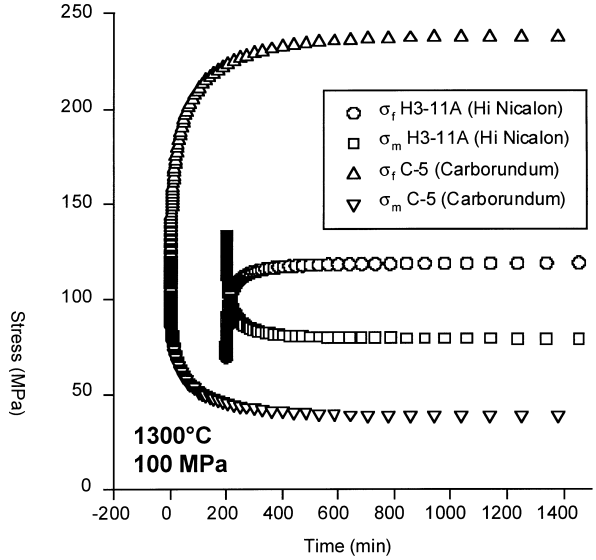

Fig. 4. Evolution of fiber and matrix stresses during microcomposite creep at 100 MPa and 1300 °C calculated from the rule of mixtures model. The Hi Nicalon microcomposite results have been shifted 200 min for clarity.

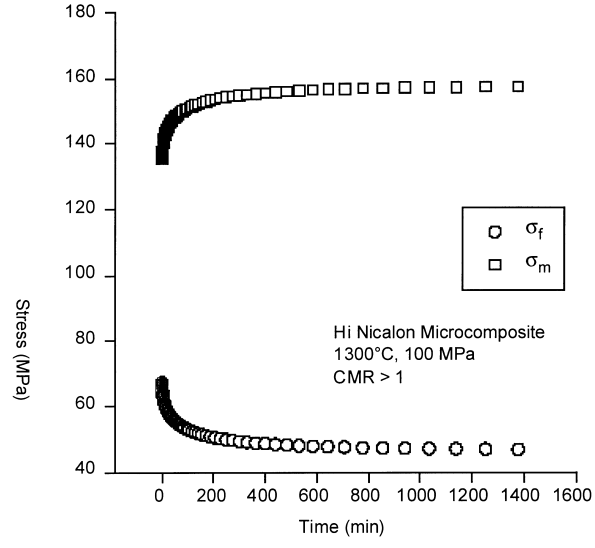

Fig. 5. Calculated fiber and matrix stresses for a Hi Nicalon-based microcomposite for which CMR > 1.

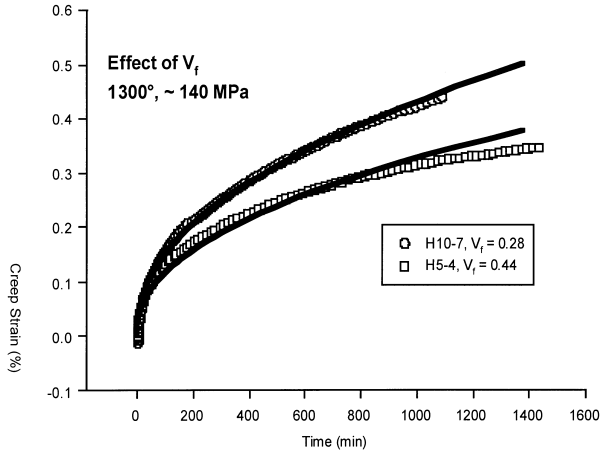

Fig. 6. Creep curves for Hi Nicalon-based microcomposites showing effect of fiber volume fraction at 1300 °C and approximately 140 MPa. The solid lines represent the prediction from the rule of mixtures model.

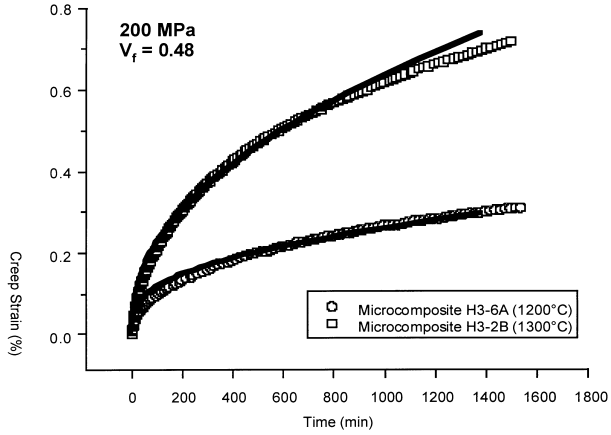

Fig. 7. Effect of temperature on the creep strain accumulation of Hi Nicalon-based microcomposites tested at 200 MPa. The solid lines represent the fits to the rule of mixtures model.

the better creep resistance. The V_f value affects both the initial and later stages of the creep curve. For smaller V_f, the matrix has a greater share of the applied stress on loading, therefore there is more creep strain initially as the elastic stress mismatch is relaxed. At longer times the fiber carries most of the load. In the limit of a matrix that carries no load, the fiber stress would go to σ_{app}/V_f. Therefore a microcomposite with a smaller V_f will have a higher fiber stress at long times and therefore have a faster creep rate. It can clearly be seen in Fig. 6 that the microcomposite with the smaller fiber volume fraction (H10-7) creeps more initially and has a higher creep rate at longer times than does the microcomposite with the larger V_f (H5-4). The rule of mixtures results for both microcomposites are shown in the figure. Again, the model correlates well with the observations.

The temperature dependence of the creep of Hi Nicalon-based microcomposites at 200 MPa is illustrated in Fig. 7. The fiber volume fraction for both specimens is 0·48. The creep rate is higher at the higher temperature as is expected. There is an important difference in the load sharing within the composite however. The calculated evolution of the stress on the fiber is plotted in Fig. 8. The stress transfer rate is slightly faster at the higher temperature, but it ceases at a much more evenly balanced load sharing condition. The activation energy for creep of the matrix is lower than that for the fiber, therefore the difference in creep rates for the two composite constituents is greater at lower temperatures. It is this difference in creep rates that induces stress transfer.

The creep curves for several Hi Nicalon-based microcomposites at different stresses are shown in Fig. 9. The rule of mixtures model works well except for specimen H3-12 which was tested at 450 MPa and 1200 °C. This discrepancy probably

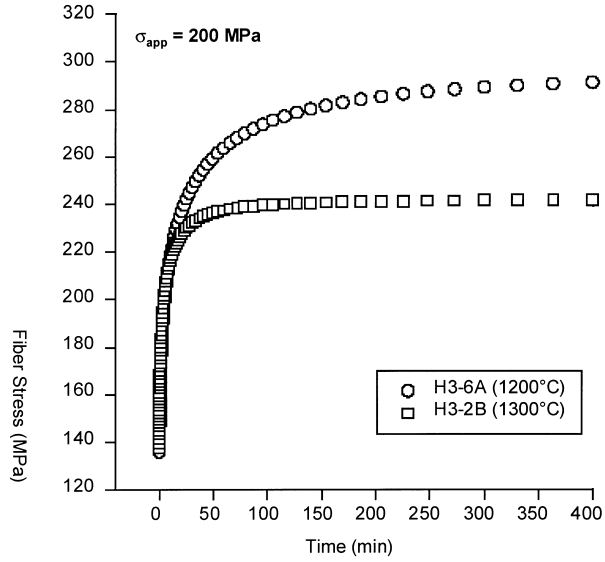

Fig. 8. Calculated evolution of fiber stress at 1200 and 1300 °C at 200 MPa and $V_f = 0{\cdot}48$ for Hi Nicalon-based microcomposites.

arises from the extrapolation of the matrix creep behavior to the high stresses experienced in this experiment. The rule of mixtures model calculates that σ_m changes from an initial value of 580 to 211 MPa at the conclusion of the experiments. The matrix creep results clearly indicate that the matrix cannot sustain this level of stress at this temperature.[23] It is possible there was undetected matrix damage for this specimen.

3.2 Creep of microcomposites with matrix cracks

Cracking of the matrix changes the stress state in the composite in the region where the fiber/matrix interface debonds.[28–30] The microcomposite creep rate increases due to the inability of the matrix to carry load in the debonded region. The fiber is under a higher stress in that region relative to that in the uncracked microcomposite.

A schematic section of a microcomposite near a matrix crack is shown in Fig. 10. The microcomposite can be broken up into three regions as indicated in the figure. In region 1, the fiber is completely debonded from the matrix and carries a stress, σ_1, equal to σ_{app}/V_f. In region 3, the microcomposite is intact. The stress on the fiber, σ_3, is dictated by stress transfer due to creep rate mismatch between the fiber and matrix as in an uncracked microcomposite. As shown previously, the fiber stress in this region increases with creep time. In region 2, the interface is debonded. The stress on the fiber in this region (σ_2) is set by the interfacial sliding resistance and is assumed to change linearly with distance, x, and is calculated from

$$\begin{aligned}\sigma_2(x,t) &= -\frac{2\tau}{R}(x - L_d) + \sigma_3(t) \\ &= -\frac{2\tau}{R}x + \sigma_1\end{aligned} \tag{4}$$

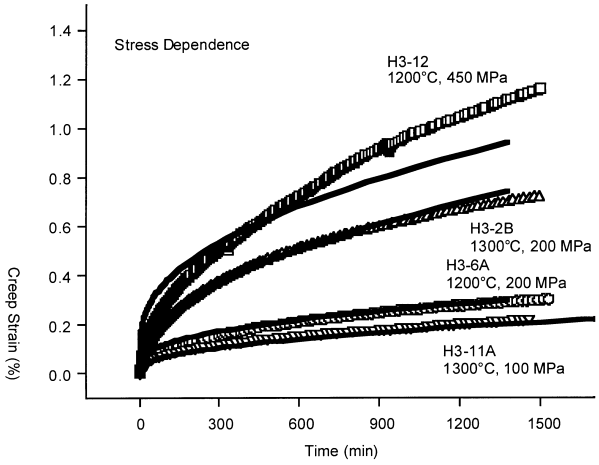

Fig. 9. Creep curves of Hi Nicalon-based microcomposites showing the stress dependence of the creep behavior.

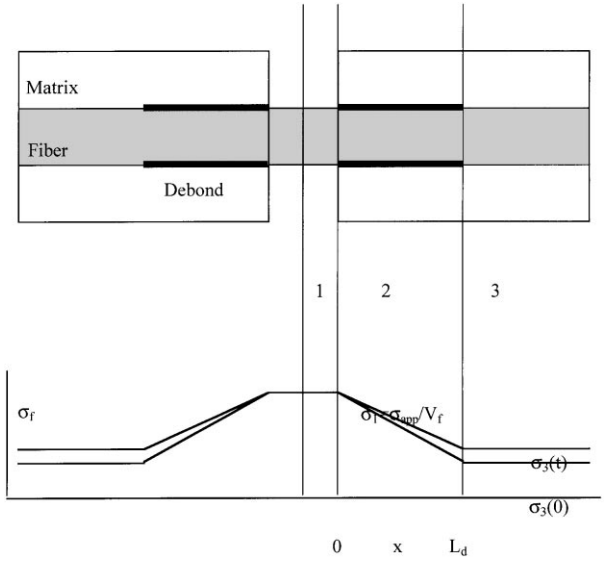

Fig. 10. Schematic of a microcomposite near a matrix crack showing the level of stress in the fiber.

where $x = 0$ at the matrix crack, R is the fiber radius, and τ is the interfacial shear stress. In this equation, the time dependence arises from the time dependence of σ_3 as derived from the rule of mixtures algorithm. If the debond does not propagate, there is a change in τ which results in a decrease in the slope of the σ_2 versus x line with time as indicated in the figure. (Propagation of a debond would also result in a decrease in τ.[13]) At $x = 0$, σ_2 will remain constant throughout the creep test at a value of σ_1. Theoretically, there is a step in the fiber stress at the debond tip[29,30] which has been ignored in the current analysis. This step is related to the fracture energy of the debond which has been shown to be very low for similar microcomposites.[22,31]

The overall creep strain of the microcomposite is the summation of the creep strains, ε_i, from each of the three regions, i.e.

$$\varepsilon(t) = \varepsilon_1(t)\frac{L_1}{L} + \varepsilon_2(t)\frac{L_2}{L} + \varepsilon_3(t)\frac{L_3}{L} \tag{5}$$

where ε_i represents the creep strain accumulated if the whole microcomposite consisted of region i, L is the total gauge length, and the $\frac{L_i}{L}$ are the fractional lengths of each region along the gauge length microcomposite. The value of ε_3 is determined from the creep behavior of an uncracked microcomposite (rule of mixtures model). The strain in region 1 is simply the fiber creep strain for a fiber creeping at $\sigma_1 = \sigma_{app}/V_f$. The value of ε_2 is also determined from the fiber creep equation, but the stress is not constant over the length of this region and changes with time. The strain increment at any time interval Δt is calculated from the integral

$$\begin{aligned}\Delta\varepsilon_2 &= \frac{\Delta\sigma_2}{E_f} + \frac{2}{L_d}\int_0^{L_d} A\sigma_2^n t^P e^{-pQ/RT}\mathrm{d}x \\ &= \frac{\Delta\sigma_2}{E_f} + \frac{2A}{L_d}\int_0^{L_d}\left[\sigma_1 - \frac{2\tau}{R}x\right]^n \mathrm{d}x\end{aligned} \tag{6}$$

where A, n, p, and Q are the fiber creep parameters, $\Delta\sigma_2$ is the change in the average stress in the debond region over the time increment, A' incorporates the time and temperature dependence of the creep rate, and $2L_d$ is the length of both debonds in the unit cell (Fig. 10). Equation (6) can be simplified to

$$\Delta\varepsilon_2 = \frac{\Delta\sigma_2}{E_f} + \frac{A'R}{2\tau(t)L_d(n+1)}\left[\sigma_1^{n+1} - \sigma_3^{n+1}\right] \tag{7}$$

Since $\Delta\varepsilon_1 = A'(t)\sigma_1^n$, the strain accumulated in region 2 during any time interval is proportional to the strain accumulated in region 1 during the same

interval plus the elastic strain derived from the change in σ_2, i.e.

$$\Delta\varepsilon_2 = \frac{\Delta\sigma_2}{E_f} + C\Delta\varepsilon_1 \tag{8}$$

where

$$C = \frac{R\sigma_1}{2\tau L_d(n+1)}(1 - B^{n+1}) \tag{9}$$

with $B = \sigma_3/\sigma_1$. It is important to remember that C, B, and τ each has a time dependence which arises from the time dependence of σ_3.

Computation of the lengths L_1, L_2, and L_3 requires knowledge of the debond length and the number of matrix cracks, N. If the shear sliding resistance of the interface is known, the debond length can be calculated from[32]

$$L_d = \frac{\sigma a R}{2V_f(1+a)(I - L_0/L_d)(\tau_0 + k\sigma)} \tag{10}$$

where $a = E_m V_m / E_f V_f$, L_0 is the distance along which the Poisson's effect is dominant and there is no stress transfer across the interface, and k is a coefficient accounting for stress dependent fiber/matrix interactions along the debond. For a first approximation it was assumed that $k = 0$ and $L_0 = 0$. The shear stress of the interface is known from the hysteresis loop measurements.[20] It is assumed that L_d does not change during creep in inert environments. Once the debond length is known, calculation of the lengths of the three regions of microcomposite is straightforward. Assuming that none of the debonds overlap,

$$\begin{aligned} L_1 &= \Sigma_N(\mathrm{COD}) \\ L_2 &= 2NL_d \\ L_3 &= L - L_1 - L_2 \end{aligned} \tag{11}$$

where COD is the average crack opening displacement. For purposes of creep modeling it is assumed that COD and L_d are equal for all cracks along the length of the microcomposite.

To make the microcomposite creep experiments practical, the specimens were precracked at a high stress, σ_{pre}. This allowed the initiation of multiple matrix cracks under conditions where the fiber is not subject to creep fatigue processes. Large diameter microcomposites were precracked by bending around a 6·5 mm diameter post rather than in a tensile test which would have caused failure of the microcomposite on first matrix cracking due to the high matrix volume fraction. The creep test can then be carried out at lower stresses. This procedure causes uncertainty about what debond length to use in the analysis of eqns (11). Upon partial reloading (applying the creep stress) fiber-matrix sliding does not occur along the entire debond length, but halts at a length L_d'[33] This length quickly increases with increasing stress on the fiber due to creep of the matrix until it reaches the end of the physical debond at which point the fiber stress profile is that depicted in Fig. 10. For simplicity of the calculations, the value of L_d used is that determined by precracking and eqn (10). It is recognized that this may lead to a small overestimation of the microcomposite creep strain (by increasing L_2) but it is likely to have a strong effect on only the initial part of the creep curve. Later in the experiments, the fiber stress is high in region 3 and sliding occurs along the entire debond length.

The observed creep rates for matrix cracked microcomposites are higher than those for intact microcomposites, as expected. The creep curve for microcomposite H3–7B is shown in Fig. 11. The curve for microcomposite H3–6A is shown for comparison. Both specimens were tested at 1200 °C and 200 MPa but microcomposite H3–7B had been precracked in tension at 900 MPa at room temperature so that there were seven matrix cracks. Specimen H3–7B also had a slightly larger fiber volume fraction. Also shown in the figure are the results of the rule of mixtures and cracked composite models. The later model is shown for two values of τ, the general value of 10 MPa and the value measured for that specimen during precracking of 14 MPa. These two shear strengths are difficult to distinguish using hysteresis loop measurements,[20] but have an important effect on the cracked composite creep model as shown.

The model works for specimens H5-9 and H5-11 as well for $\tau = 10$ MPa and assuming $N = 2$ for H5-11. The creep curve for H5-9 is shown in Fig. 12. The microcomposite failed after 9·8 h at 1300 °C and 381 MPa.

In order to demonstrate the influence of the different parameters that control the creep of

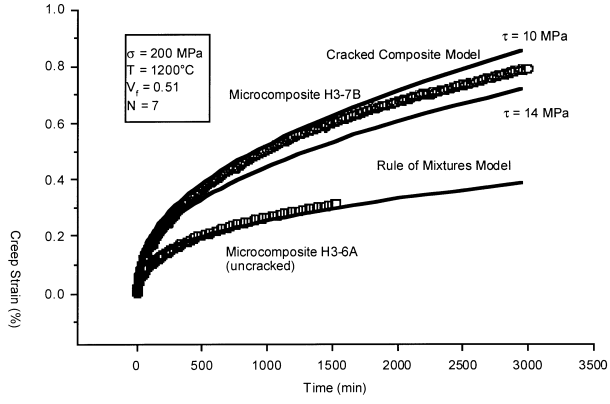

Fig. 11. Comparison of the creep of cracked and uncracked Hi Nicalon-based microcomposites at 1200 °C and 200 MPa. The results of the rule of mixtures and cracked composite creep models are shown by the solid lines.

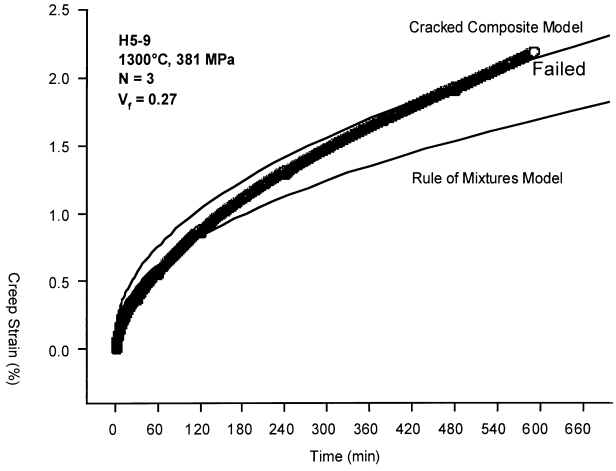

Fig. 12. Creep curve for microcomposite H5-9 tested at 1300 °C and 381 MPa.

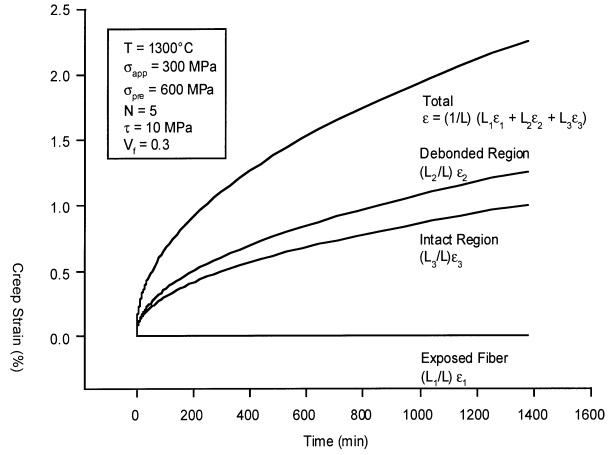

Fig. 13. The creep curves for each region of a matrix cracked microcomposite normalized to its relative gauge length. The creep strain for the microcomposite is the sum of that for each of the three regions.

microcomposites having matrix cracks, a series of calculated creep curves for Hi Nicalon microcomposites tested at generic creep conditions are presented. Each plot highlights the effect of one of the key variables. The baseline parameters used to generate these plots are $\sigma_{pre} = 600$ MPa, $\sigma_{app} = 300$ MPa, $T = 1300\,°C$, $V_f = 0{\cdot}3$, $R = 7\,\mu$m, $\tau_0 = 10$ MPa, and $N = 5$. The crack opening displacement ($= L_1/N$) is taken as $1\,\mu$m. The stress parameters yield a debond length of $576.5\,\mu$m and an initial τ (at the creep stress) of 5·34 MPa. The values of L_1/L, L_2/L, and L_3/L are 0·033, 38·4, and 61·6%, respectively.

The creep curves calculated for each region of the microcomposite, normalized to its relative gauge length are plotted in Fig. 13. It is apparent that the largest contribution to the overall creep strain (55·6% at $t = 24$ h) comes from the debonded region (region 2) of the microcomposite, despite its length being shorter than that of the intact section. Although the creep rate of the microcomposite is fastest at the crack opening, the small length of that region makes its contribution to the overall creep strain negligible. Increasing the assumed crack opening by an order of magnitude to $10\,\mu$m contributes only an additional 0·015% to the total creep strain. As a result, the creep in region 1 can be disregarded in the microcomposite creep model.

The interfacial shear stress has a strong influence on the creep behavior of the cracked microcomposite. The creep curves for $\tau = 5$, 10, 25, and 100 MPa (at precracking) are shown in Fig. 14. It has been shown that the number of matrix cracks is dependent on the interfacial stress,[32] but for this analysis N is assumed to be constant. The effect of a small change in shear stress is more important at low values of τ. Doubling τ from 5 to 10 MPa decreases the strain accumulated in 24 h (1440 min) by 21·7% while increasing τ a factor of 4 from 25 to 100 MPa results in only a 9·6% change in strain.

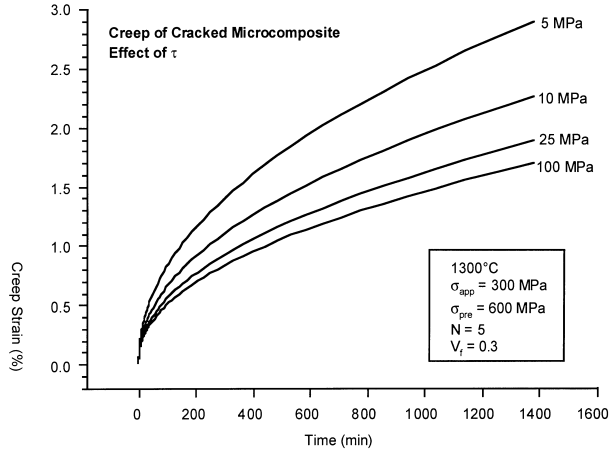

Fig. 14. Effect of the interfacial strength on the creep of cracked microcomposites.

The differences in creep accumulation with τ result from the variation in debond length with shear stress. By eqn (10), the debond length is inversely proportional to the interfacial shear stress. At a shear stress of 5 MPa, the debond length is $1153\,\mu$m for the experimental conditions assumed. For a shear stress of 10 MPa, the debond length decreases to $577\,\mu$m. The portion of the microcomposite in region 2 drops from 76·9% at $\tau =$ 5 MPa to 38·4% at $\tau = 10$ MPa. The values of L_2 for $\tau = 25$ and 100 MPa are 15·4 and 3·8%, respectively. The stresses along the debond vary over the same range from $\sigma_3(t)$ to σ_1 for all four values of the shear strength, but the distance they are acting over changes significantly.

If toughening is to be achieved by fiber pull out, weak fiber/matrix bonding (low τ) is needed.[22] Alternatively, high toughness can be achieved with a strong interface if a dense network of matrix cracks can be generated.[32] For the same number of matrix cracks, the Hi Nicalon microcomposite with the strongest interface will creep the least as shown

in Fig. 14. In other systems (see below for Carborundum microcomposites) the effect may not be as important. Increasing τ, however, can result in increased matrix cracking.[32] Overall, high values of τ may be preferable since composites with strong interfaces favor high applied stresses and a high stress at matrix crack saturation relative to the weak interface case.[32]

The calculated creep curves for different fiber volume fractions are shown in Fig. 15. The fiber volume fraction affects the microcomposite creep behavior in several different ways. At lower V_f, the stress on the fiber at the matrix crack is higher, therefore the stress in the debond is higher and the creep rate is higher. As shown in Fig. 6, decreasing the fiber volume fraction increases the creep rate in region 3 of the cracked microcomposite. The calculated debond length also changes with volume fraction as indicated by eqn (10). The debond length is 933·3 μm for $V_f = 0{\cdot}2$, 576·5 μm for $V_f = 0{\cdot}3$, and 280 μm for $V_f = 0{\cdot}5$. The change in debond length means that significantly more of the microcomposite is in region 2 as the volume fraction decreases.

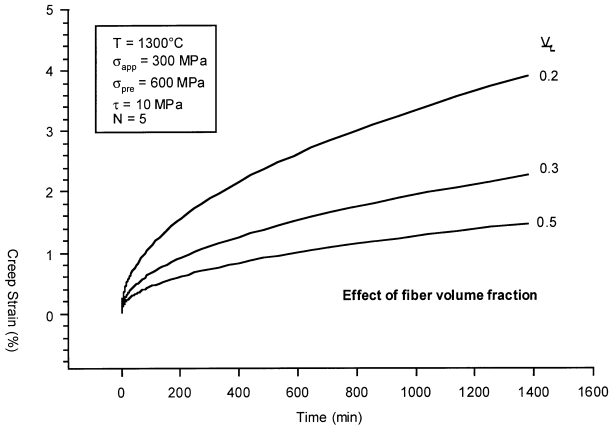

Fig. 15. Calculated creep curves for cracked microcomposites with different fiber volume fractions.

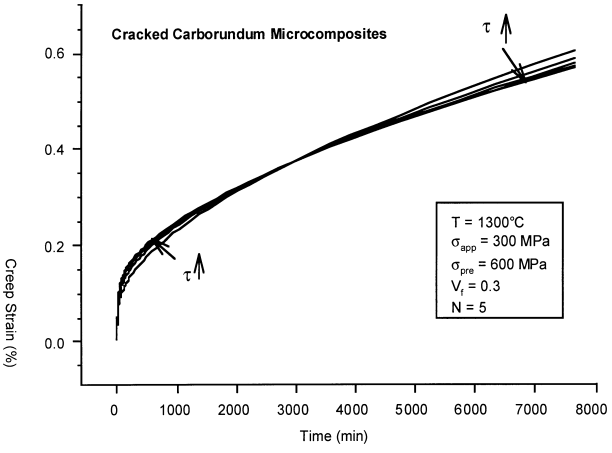

Fig. 16. Predicted creep behavior of matrix cracked Carborundum-based microcomposites showing effect of interfacial shear strength.

The sensitivity of the creep curve to creep temperature and applied stress is similar to those for the uncracked microcomposite and will not be discussed further here. Increasing the precracking stress produces additional matrix cracks and longer debonds if the fiber/matrix interface cracks grow, thereby increasing the relative length of region 2 of the microcomposite. Since creep is faster in region 2 than in region 3, the overall creep rate will be higher.

The trends described above for the creep of matrix cracked microcomposites hold for all systems with a CMR less than one. Fig. 16 shows the effect of replacing the Hi Nicalon fiber in the model microcomposite with the more creep resistant Carborundum fiber. The creep curves shown in the figure are not realistic since the Carborundum fiber is known to undergo subcritical crack growth at the creep temperature.[34] Failure would occur rapidly for the conditions in the figure since the fiber stress at the matrix cracks is 1 GPa. The figure is used only to illustrate the trends expected for a more creep resistant fiber.

Since interfacial sliding was not observed for Carborundum-based microcomposites, the interfacial strength is unknown, therefore the creep behavior is plotted for several values of τ: 5, 10, 25, and 100 MPa. At $\tau = 100$ MPa, the calculated creep behavior is barely distinguishable from that of an intact microcomposite. It should be recognized that the surface of the Carborundum fiber is very rough, therefore a high value of the sliding resistance is expected, so the behavior may be that for the $\tau = 100$ MPa case. As is clear in the figure, matrix cracking has less of an effect on the Carborundum-based microcomposite than it did for the Hi Nicalon microcomposite. The value of the CMR for the Carborundum-based microcomposite is lower than for Hi Nicalon composites. Since the fiber creeps less than the Hi Nicalon fiber, it takes more stress from the matrix in region 3 as was demonstrated in Fig. 4. As a result, the creep rate in region 3 is much closer to that in region 2 for the Carborundum microcomposite. Therefore, the change in creep rate for the Carborundum microcomposite due to matrix cracking is relatively low, particularly for a small number of cracks.

An interesting feature of Fig. 16 is that for relatively long times (~40 h) there is less creep strain for the cracked Carborundum-based microcomposite than for the uncracked microcomposite. This results from the same effect that was shown in

Fig. 2 where a fiber tested at σ_{app}/V_f creeps less than the uncracked microcomposite. In the cracked microcomposite, there is less elastic strain of the fiber during creep resulting from relaxation of matrix stress. The fiber stress in region 3 of the microcomposite changes twice as much as the average fiber stress in region 2 according to Fig. 4. Since the creep of a Carborundum fiber is slow at 1300 °C, the time necessary to overcome the resulting strain difference is long. It can be seen in the figure that the creep rates of the cracked microcomposites are higher after the stress transfer period, and the creep curves do eventually cross. It should be remembered that this discussion pertains to creep strain, not total strain. The presence of matrix cracks causes more strain during loading. If Fig. 16 showed total strain rather than creep strain, the matrix cracked specimens would always be at higher strains.

The previous analyses have been for a CMR < 1, but the model can also be used for CMR > 1 assuming that the debond length does not grow. The calculated creep curves for Hi Nicalon microcomposites with and without matrix cracks for two different matrix creep rates are shown in Fig. 17. The lower matrix creep parameters were generated by dividing the observed matrix creep behavior by a factor of 10. This procedure provides CMR > 1. The effect of matrix cracking is much greater for the microcomposite with CMR > 1. The creep strain is 241% greater at the finish of the creep curve for the matrix cracked microcomposite when CMR > 1. For the original calculation, the difference is only 39%. As shown in Fig. 5, the fiber stress decreases during the creep of the CMR > 1 microcomposite. Therefore, the difference between the fiber stresses in regions 2 and 3 of the microcomposite is much greater than for the CMR < 1 specimen. The difference in creep rates between region 2 and region 3 is greater resulting in the larger creep strains.

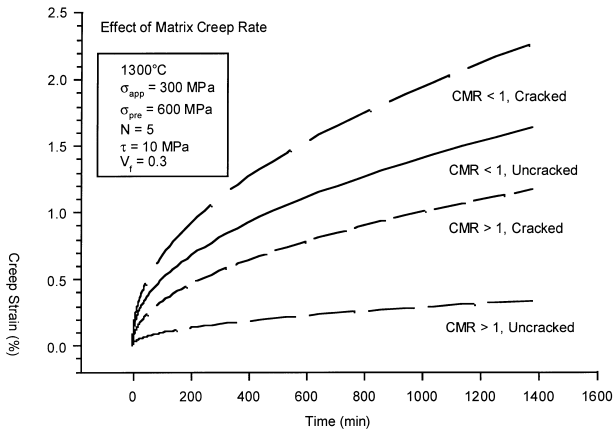

Fig. 17. Comparison of creep models for microcomposites with CMR > and < 1.

4 Conclusions

The creep behavior of SiC–SiC microcomposites was measured and modeled at 1200–1300 °C and 100–450 MPa. Two creep models were presented differing by the absence or presence of matrix cracking:

1. In the absence of matrix cracking, the microcomposite creep behavior can be described by a simple rule of mixtures model which predicts rapid stress transfer from the less creep resistant matrix to the more creep resistance fibers.
2. After matrix cracking, the microcomposites can be split into three sections: the intact region, the exposed fiber at the crack, and the debonded section in between. By weighting the creep strain in each of these sections by its relative length, the total creep behavior of the microcomposite is obtained.

The models were shown to be consistent with the observed microcomposite creep strain for different fiber creep rates, volume fractions, ambient temperatures, and applied stresses. Using these models, the creep behavior for a theoretical composite system can be described given the creep mismatch ratio and the interfacial shear strength.

References

1. Chermant, J. L. and Holmes, J., Elevated temperature creep and cyclic creep behavior of fiber-reinforced ceramics. In *High Temperature Ceramic-Matrix Composites I*, ed. A. G. Evans and R. Naslain. American Ceramic Society, Westerville, OH, 1995, pp. 95–106.
2. Grathwohl, G., Meier, B. and Wang, P., Creep of fiber and whisker reinforced ceramics, glass-ceramics, and glasses. *Key Eng. Mat.*, 1995, **108–110**, 243–268.
3. Hill, B. B., Bakis, C. E. and Hahn, H. T., Creep of SiC/RBSN composite: analytical modeling. In *Constitutive Behavior of High-Temperature Composites*, ed. B. S. Newaz, G. M. Newaz and S. Mall. ASME, New York, 1992, pp. 121–135.
4. Park, Y. H. and Holmes, J. W., Finite element modeling of creep deformation in fibre-reinforced ceramic composites. *J. Mat. Sci.*, 1992, **27**, 6341–6351.
5. Holmes, J. W., Park, Y. H. and Jones, J. W., Tensile creep and creep-recovery behavior of a SiC–fiber–Si_3N_4-matrix composite. *J. Am. Ceram. Soc.*, 1993, **76**(5), 1281–1293.
6. Abbe, F., Vicens, J. and Chermant, J. L., Creep behavior and microstructural characterization of a ceramic matrix composite. *J. Mat. Sci. Let.*, 1989, **8**, 1026–1028.
7. Abbe, F., Carin, R. and Chermant, J. L., Tensile and compressive creep characteristics from bending tests: application to SiC–SiC composites. *J. Eur. Ceram. Soc.*, 1989, **5**, 201–205.
8. Kervadec, D., Abbe, F. and Chermant, J. L., Steady state creep behavior of two ceramic composites SiC_f–SiC and SiC_f–MLAS. *J. Phys. IV*, 1993, **3**, 1917–1922.
9. Mozdzierz, N. and Backhaus-Ricoult, M., High temperature creep performance and microstructure of SiC–C–SiC composites. *J. Phys. IV*, 1993, **3**, 1931–1936.
10. Lamouroux, F., Steen, M. and Vallés, J. L., Uniaxial tensile and creep behavior of an alumina fibre-reinforced

ceramic matrix composite: I. Experimental study. *J. Eur. Ceram. Soc.*, 1994, **14**, 529–537.
11. Evans, A. G. and Weber, C., Creep damage in SiC/SiC composites. *Mat. Sci. Eng. A*, 1996, **A208**, 1–6.
12. McLean, M., Creep deformation of metal-matrix composites. *Comp. Sci. Tech.*, 1985, **23**, 37–52.
13. Lamouroux, F., Vallés, J. L. and Steen, M., Uniaxial tensile and creep behavior of an alumina fibre-reinforced ceramic matrix composite: II. Modelling of tertiary creep. *J. Eur. Ceram. Soc.*, 1994, **14**, 539–548.
14. Lara-Curzio, E. and Ferber, M. K., Some considerations for modelling the creep behavior of composite materials. *Ceram. Eng. Sci. Proc.*, 1994, **15**(4), 65–75.
15. Strait, S. J., Bakis, C. E., Lewinsohn, C. A. and Tressler, R. E., Deformation of CVD silicon carbide monofilaments under variable mechanical loading. *Ceram. Eng. Sci. Proc.*, 1994, **15**(4), 198–205.
16. El-Azab, A. and Ghoniem, N. M., Time-dependent micro-mechanics in damaged high-temperature ceramic composites. *ASME AMD*, 1995, **199**(55), 23–38.
17. Lara-Curzio, E. and Sternstein, S. S., Thermoelastic analysis of composite CVD SiC fibers. *Comp. Sci. Tech.*, 1993, **46**, 265–275.
18. Lamon, J., Rebillat, F. and Evans, A. G., Microcomposite test procedure for evaluating the interface properties of ceramic matrix composites. *J. Am. Ceram. Soc.*, 1995, **78**(2), 402–405.
19. Morsher, G. N., Fernandez, J. M. and Purdy, M. J., Determination of interfacial properties using a single fiber microcomposite test. *J. Am. Ceram. Soc.*, 1996, **79**(4), 1083–1091.
20. Rugg, K. L., Tressler, R. E. and Lamon, J., Interfacial behavior of microcomposites at elevated temperatures. *Euro. Ceram. Soc.*, 1999, **19**(13–14), this issue.
21. Begley, M. R., Cox, B. N. and McMeeking, R. M., Time dependent crack growth in ceramic matrix composites with creeping fibers. *Acta Metall. Mater.*, 1995, **43**(11), 3927–3936.
22. Lamon, J., Rechiniac, C., Lissart, N. and Corne, P., Determination of interfacial properties in ceramic matrix composites using microcomposite specimens. In *Proceedings of the 5th European Conference on Composite Materials*, ed. Bunsell *et al.* EACM-CEC, Bourdeaux, France, 1992, p. 585.
23. Rugg, K. L. and Tressler, R. E., Comparison of the creep behavior of silicon carbide fibers. In *Advances in Ceramic Matrix Composites III*, ed. N. P Bansal and J. P. Singh. The American Ceramic Society, Westerville, OH, 1996, pp. 27–36.
24. Rugg, K. L., Mechanical behaviour at high temperatures of single fiber microcomposites, Ph.D. Thesis, The Pennsylvania State University, 1999.
25. Pysher, D. J., Giannuzzi, L. A. and Tressler, R.E., An apparatus for mechanically testing single filaments at high temperature in a controlled atmosphere or vacuum. *Rev. Sci. Instruments*, submitted for publication.
26. Jia, N., Bodet, R. and Tressler, R. E., Effect of microstructural instability on the creep behavior of Si–C–O (Nicalon) fibers in argon. *J. Am. Ceram. Soc.*, 1993, **76**(12), 3051–3060.
27. DiCarlo, J. A., Yun, H. M., Morsher, G. N. and Goldsby, J. C., Models for the thermostructural properties of SiC fibers. In *High Temperature Ceramic Matrix Composites II* (HT-CMC-2), ed. R. Naslain and A. G. Evans. American Ceramic Society, Westerville, OH, 1995, pp. 343–348.
28. Evans, A. G. and Zok, F. W., Review. The physics and mechanics of fibre-reinforced brittle matrix composites. *J. Mat. Sci.*, 1994, **29**, 3857–3896.
29. Hutchinson, J. W. and Jensen, H. M., Models of fiber debonding and pullout in brittle composites with friction. *Mech. Mat.*, 1990, **9**, 139–163.
30. Marshall, D. B., Analysis of fiber debonding and sliding experiments in brittle matrix composites. *Acta Metall. Mater.*, 1992, **40**(3), 427–441.
31. Lamon, J., Lissart, N., Rechiniac, C., Roach, D. H. and Jouin, J. M., Micromechanical and statistical approach to the behavior of CMC's. *Cer. Eng. Sci. Proc.*, 1993, **14**(9–10), 1115–1124.
32. Guillamat, L. and Lamon, J., Fracture statistics applied to modelling the nonlinear stress–strain behavior in microcomposites: influence of interfacial parameters. *Int. J. Fract.*, 1996, **82**, 297–316.
33. Vagagginni, E., Domergue, J. M. and Evans, A. G., Relationships between hysteresis measurements and the constituent properties of ceramic matrix composites: I, theory. *J. Am. Ceram. Soc.*, 1995, **78**(10), 2709–2720.
34. Tressler, R. E., Rugg, K. L., Martz, S. W., Sglavo, V. M. and Newcomb, S. A., Delayed failure of ceramic fibers at elevated temperatures. In *High Temperature Ceramic Matrix Composites I* (HT-CMC-2), ed. R. Naslain and A. G. Evans. American Ceramic Society, Westerville, OH, 1995, pp. 375–380.